Int. J. Electrochem. Sci., 6 **(2011)** 78 - 90

International Journal of
ELECTROCHEMICAL
SCIENCE
www.electrochemsci.org

Characterization of Composite Mesoporous Carbon/Conducting Polymer Electrodes Prepared by Chemical Oxidation of Gas-Phase Absorbed Monomer for Electrochemical Capacitors

D.E. Pacheco-Catalán[1,2,*], *Mascha A. Smit*[2], *E. Morales*[1]

[1] Instituto de Ciencia y Tecnología de Polímeros CSIC, c/ Juan de la Cierva 3, 28006 Madrid, Spain.
[2] Unidad de Energía Renovable, Centro de Investigación Científica de Yucatán A.C., C.P. 97200, Mérida, Yucatán, México.
[*]E-mail: mascha@cicy.mx

Received: 11 October 2010 / *Accepted:* 30 October 2010 / *Published:* 1 January 2011

Mesoporous carbon/conducting polymer composites have been synthesized by adsorption of different monomers (aniline, pyrrole, thiophene and 3-methyltiophene) in the gas phase onto the carbon surface, followed by oxidative chemical polymerization. The materials were tested as electrode material for electrochemical capacitors. The pore structure of the composites was examined by N_2 isotherm adsorption at low temperature, showing that the synthesis of the polymers onto the carbon leads to a decrease of the BET surface value and the pore volume. The pore size distribution was unaltered independently of the polymer nature and concentration. Electrochemical performance of the composites was studied by cyclic voltammetry, galvanostatic charge/discharge, and electrochemical impedance spectroscopy in 2.0 mol l^{-1} H_2SO_4. All composite electrodes show a stable cycle life in the potential range of 0 to 1V, the specific capacitance of carbon/polypyrrole composite electrode (83.8 $F \cdot g^{-1}$) being slightly higher than that obtained for the pristine mesoporous carbon electrode (77.9 $F \cdot g^{-1}$). The remaining carbon/polymer composites show lower specific capacitance than carbon only, due to their higher internal resistance (ESR).

Keywords: Conducting polymer, mesoporous carbon, supercapacitors

1. INTRODUCTION

Electrochemical capacitors, also known as supercapacitors or ultracapacitors, have been extensively investigated in recent years because of their potential application as power storage devices in applications such as electrical vehicles, portable computers, mobile devices and nanoelectronics [1-4]. These devices can combine two types of energy storage mechanism: electrosorption of ions at the electrode/electrolyte interface of highly porous materials (double layer capacitance) [1, 5] and fast

reversible redox reactions of the electrode material (pseudo-capacitance) [1, 5-7]. In the first case, the electrodes are generally based on carbon materials ranging from activated carbons (ACs) to carbon nanotubes (CNTs), while pseudocapacitors employ electrodes made from conducting polymers [5, 8-10] or metallic oxides [5, 11-14]. Today's research on electrochemical capacitors focuses on the improvement of the energy density, $E = 0.5\ CV^2$, where C and V are the capacitance and voltage, respectively. Considering that the cell voltage of a symmetric capacitor depends on the stability window of the electrolyte (around 1 V for aqueous and 2.3V for non-aqueous electrolytes) [15, 16], the improvement in energy density mainly depends on increasing capacitance.

At present most of the devices available in the market are double layer capacitors, based on high surface area active carbons. Taking into account that pseudo-capacitors can provide capacitance values of the order of 100–1000 $\mu F \cdot cm^{-2}$, much higher than that provided double layer capacitor devices (15–50 $\mu F \cdot cm^{-2}$) [17], efforts are made to enhanced the specific capacitance of carbon-based materials through nanostructured mesoporous carbons [18, 19], pseudocapacitance by introducing additional faradaic reactions, using conducting polymers [8, 9, 20], transition metal oxides [21, 22], and the presence of heteroatoms (nitrogen and oxygen) which can undergo fast redox reactions [7, 23, 24].

In this work, mesoporous carbon/conducting polymer composites, synthesized by oxidative polymerization of monomers (aniline, pyrrole, thiophene and 3-methyltiophene) adsorbed in the gas phase onto the surface of the carbon, have been tested as electrode material for electrochemical capacitors. Under these conditions, the polymer is expected to form a monolayer, without drastic changes in the pore structure of the carbon.

2. EXPERIMENTAL

Monarch 1400 mesoporous carbon was supplied by Cabot. Aniline, pyrrole, thiophene and 3-methylthiophene (Aldrich) were freshly distilled before used. The preparation of the carbon/conducting polymer composites by oxidative chemical polymerization after monomer adsorption in the gas phase inside the porous structure of the carbon was performed as follows:

The mesoporous carbon (MesoC) was dried under vacuum (180 ºC, 10^{-2} mmHg, 24 h). Monomer adsorption onto the dried mesoporous carbon takes places under vacuum at different temperatures (40 or 60 ºC, depending on the vapour pressure of the monomer) until reaching constant weight (72 h). Carbon/polyaniline (MesoC/PANI) and carbon/polypyrrole (MesoC/PPY) composites were synthesized by chemical oxidative polycondensation of the monomer using ammonium persulfate as oxidant in 0.5 M H_2SO_4 aqueous media. Carbon/polythiophene (MesoC/PT) and carbon/poly(3-methylthiophene) (MesoC/P3MT) composites were synthesized in acetonitrile medium using $FeCl_3$ as oxidant. In all cases the oxidant/monomer ratio was fixed to 4/1. Composites were obtained by filtration, washed several times with distilled water and finally dried at 80 ºC under vacuum. The mass of monomer and polymer in the composite was determined by N and S microanalysis, using a LECO CHNS932 equipment.

The porous texture of the carbon and the carbon-conducting polymer composites was characterized by nitrogen adsorption at -196.2 ºC (Micromeritics ASAP 2010). Before the analysis, the samples were degassed at 80 ºC for 72 h under vacuum (10^{-3} mmHg). The specific surface area was determined from the N_2-adsorption isotherm using the BET equation [25]. The pore volume (V_{N2}) was calculated by applying the Dubinin–Radushkevich (DR) equation to the N_2-adsorption isotherms [26]. The microporous surface area was obtained from the equation: S_{mic} ($m^2 \cdot g^{-1}$) = $2000V_{N2}$ ($cm^3 \cdot g^{-1}$)/L_0 (nm), where L_0 represents the average micropore width [27]. Additionally, the analysis of the adsorption isotherm by a classical comparison plot based on the reference N_2 adsorption for a non-porous carbon (Vulcan 3G carbon) provided information on the mesopore area, S_{meso}, and the total surface area, S_{comp}, of the samples [28-30]. The pore size distribution was calculated by means of the Kruk–Jaroniec–Sayari method [31] applied to the adsorption branch.

The electrochemical performance of the composites was analyzed in symmetric two-electrode Swagelok™-type cells by cyclic voltammetry, galvanostatic charge/discharge and impedance spectroscopy experiments using a Solartron 1480 potentiostat/galvanostat in a potential window from 0 to 1 V.

Supercapacitor electrodes were processed as cylindrical pellets of 12 mm diameter and approximately 1 mm height by cold-pressing (500 kg, 10 min) a mixture of 72 wt% of the composite, 18 wt% of PTFE binder (Aldrich) and 10 wt% of carbon black (SuperP, 3M). Each pellet contained about 40 mg of active material. The capacitors were prepared from 2 identical electrodes, separated by glassy microfibre paper discs (Whatman BS45) with aqueous 2.0 M H_2SO_4 solution as electrolyte. Two stainless steel rods (alloy A20) acted as current collectors. All cells were completely discharged before each experiment.

3. RESULTS AND DISCUSSION

Data obtained from N and S microanalysis are compiled in Table 1 (average of three tests).

Table 1. Concentration of adsorbed monomer and polymer on mesoporous carbon.

Sample	Adsorbed monomer (% w/w)	Polymer concentration (% w/w)
MesoC/PANI	23.63	2.53
MesoC/PPY	5.33	0.17
MesoC/PT	9.49	3.41
MesoC/P3MT	8.43	2.16

Results indicate that in all cases the concentration of conducting polymer in the composites was low, in the range of 0.17 wt% for MesoC/PPY to 3.41 wt% for MesoC/PT, much lower than observed for monomer adsorption, thus indicating poor carbon-monomer interactions, with diffusion of the monomer into the solution during the polymerization process.

Figure 1 shows the N_2 adsorption–desorption isotherm of the mesoporous carbon and the synthesized carbon/conducting polymer composites. In terms of shape, the isotherm for mesoporous carbon can be classified as type IV according to the IUPAC.

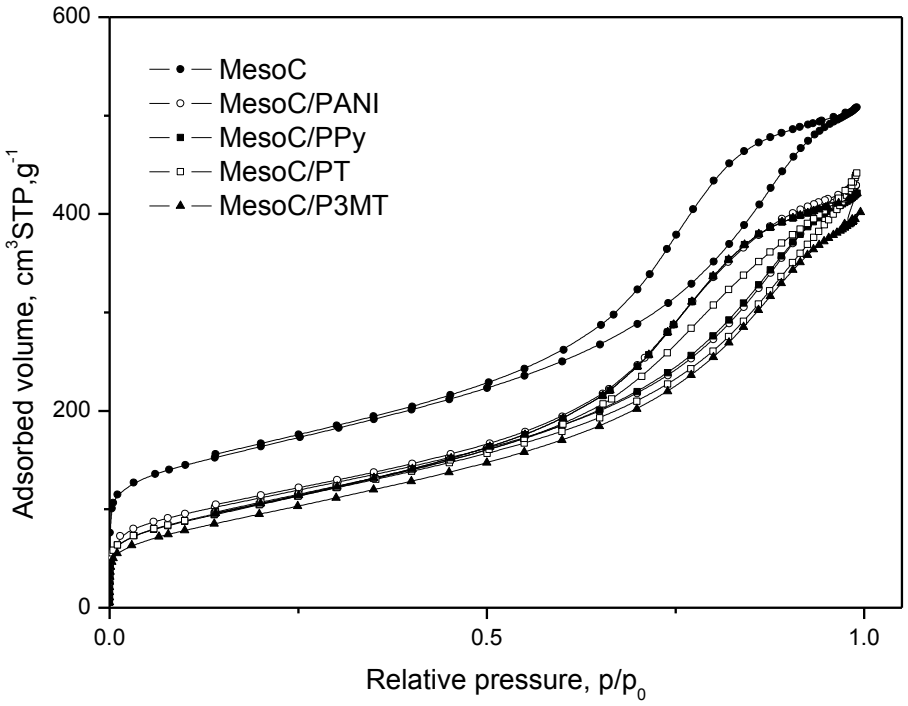

Figure 1. Adsorption/desorption isotherms of N_2 at 77 K on mesoporous carbon and synthesized carbon/conducting polymer composites.

A distinct hysteresis loop can be observed in the range of ca. 0.6–1.0 p/p_0 (p/p_0 being the relative pressure), indicating the presence of mesopores [32].

Table 2. Textural properties of carbon/conducting polymer composites.

Sample	S_{BET} ($m^2 \cdot g^{-1}$)	Total pore volume ($cm^3 \cdot g^{-1}$)	Micropore volume ($cm^3 \cdot g^{-1}$)	Micropore area ($m^2 \cdot g^{-1}$)	Mesopore volume ($cm^3 \cdot g^{-1}$)
MesoC	555	0.73	0.22	270	0.787
MesoC/PANI	396	0.68	0.15	124	0.664
MesoC/PPY	376	0.56	0.14	121	0.523
MesoC/PT	377	0.51	0.14	128	0.509
MesoC/P3MT	344	0.51	0.13	93	0.498

The carbon/conducting polymer composites show isotherms similar in shape to that obtained for the pristine carbon, differences being detected at p/p_0 close to 0 (micropore filling region). The

mesoporous carbon exhibits a specific BET surface of 555 $m^2 \cdot g^{-1}$, value that decreases for the composites, due to the filling of pores (especially the micropores) by the polymer (see Table 2 for details).

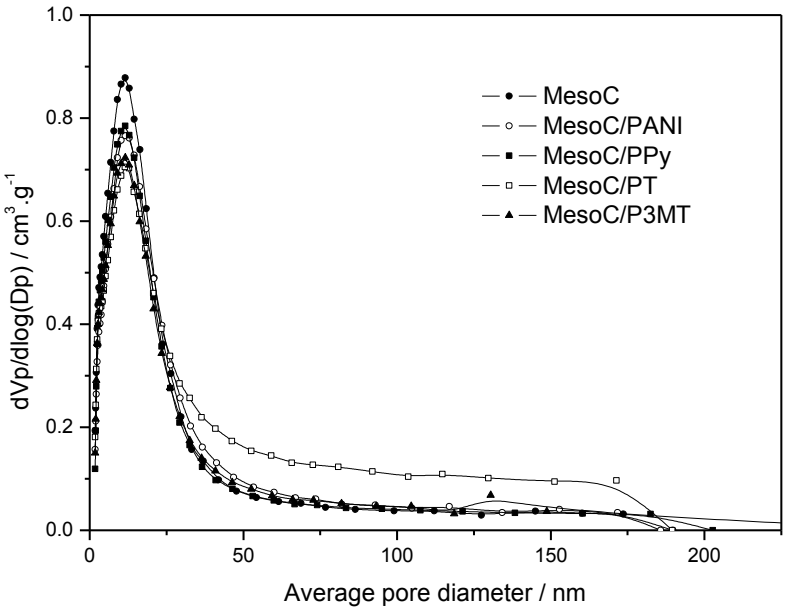

Figure 2. Pore size distribution of mesoporous carbon and the synthesized carbon/conducting polymer composites.

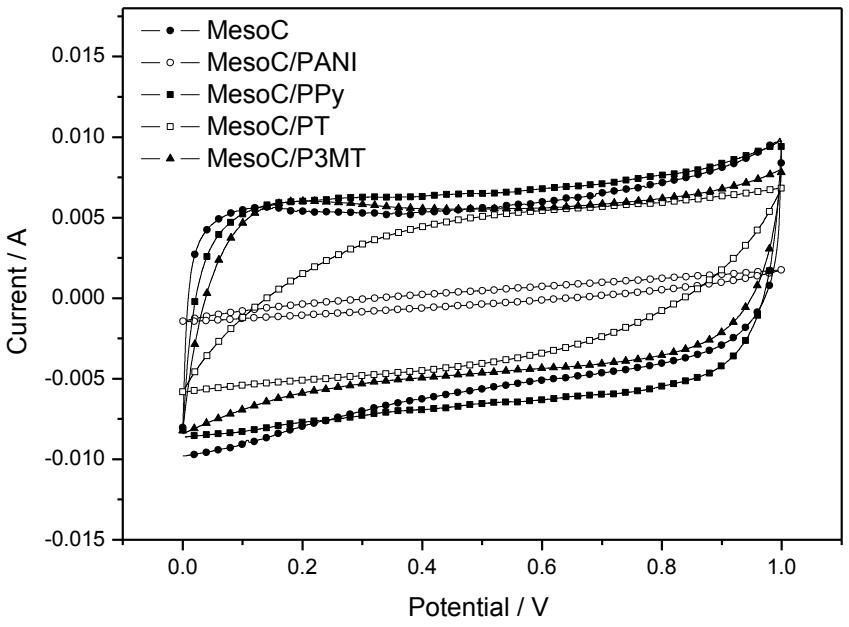

Figure 3. Cyclic voltammograms of mesoporous carbon and carbon/conducting polymer composite electrode based electrochemical capacitors. Scan rate 5 $mV \cdot s^{-1}$.

The pore distribution of the mesoporous carbon and the mesoporous carbon/conducting polymer composites is shown in Figure 2. It is clear from the graph that the incorporation of the low amount of conducting polymer to the carbon has little effect on the mesoporous structure of the carbon, the pore size being unaltered independently of the polymer nature and concentration.

Figure 3 shows the cyclic voltammograms for the electrochemical capacitors under study obtained at a 5 $mV \cdot s^{-1}$ potential scan rate. The curves corresponding to the capacitors based on the unmodified carbon, and the MesoC/PPY and MesoC/P3MT composites show nearly ideal rectangular shape at lower scan rates; at higher scan rates (~100 $mV \cdot s^{-1}$), however, the shapes deviate from the rectangular shape and an increase in current is observed at high potentials. This can be attributed to the redox processes taking place, such as the oxidation of the polymers and active groups at the carbon surface. The other two capacitors show deviations from the rectangular shape due to an increase of the internal resistance, specially the device based on the MesoC/PANI composite.

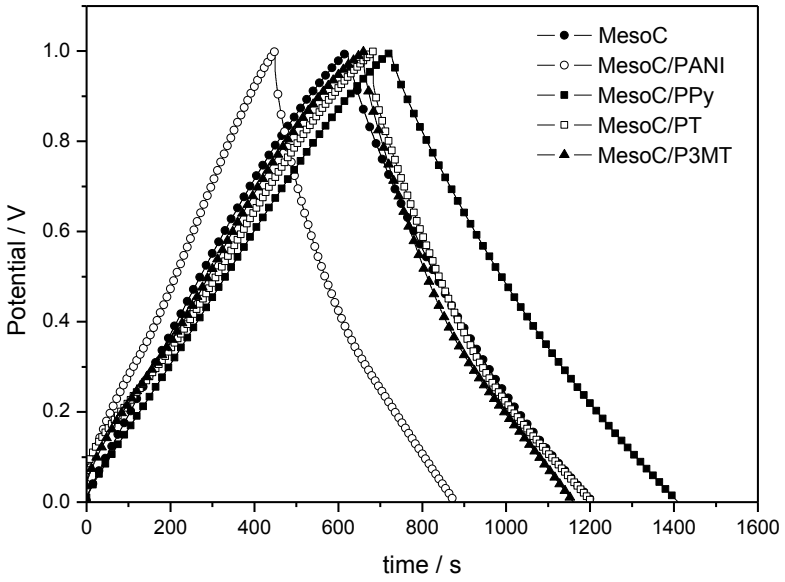

Figure 4. Galvanostatic charge-discharge curves of mesoporous carbon and carbon/conducting polymer composite electrode based electrochemical capacitors. Applied current density 2 $mA \cdot cm^{-2}$.

Galvanostatic charge–discharge curves corresponding to the different capacitors, obtained at a constant current density of 2 $mA \cdot cm^{-2}$, are shown in figure 4. From the discharge process, the capacitance of the cell can be determined as

$$C = I \cdot \frac{t_d}{\Delta V_2} \qquad (1)$$

where t_d is the time spent during discharge and ΔV_2 is the voltage range in which the discharge occurs. Since the cell is symmetrical, the specific capacitance of the electrode is calculated as two

times the cell capacitance divided by the active mass of one electrode (40 mg of active material approximately).

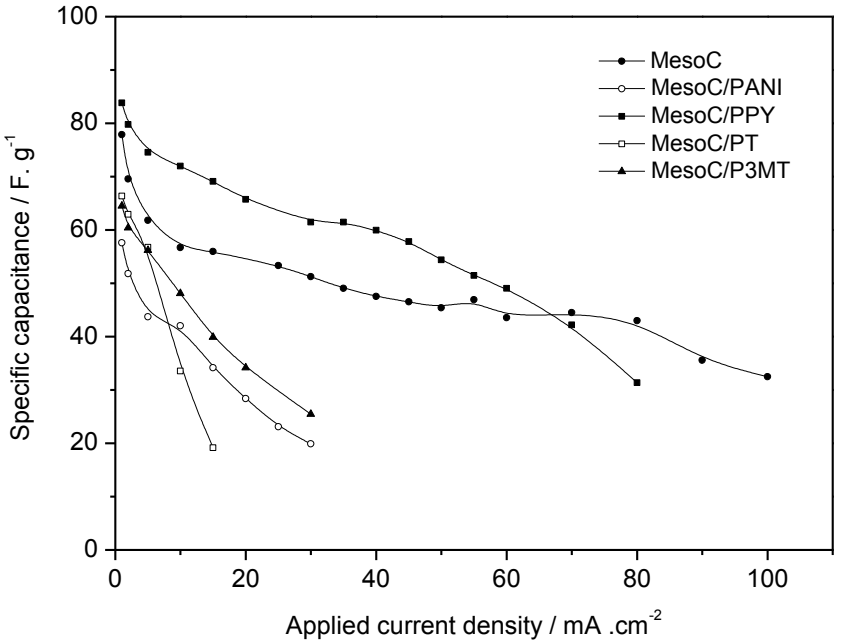

Figure 5. Discharge specific capacitance of mesoporous carbon and carbon/conducting polymer electrodes as function of applied current density.

Figure 5 shows the single electrode specific capacitance values, $C_{sp,}$ against current density. The highest value is observed for the electrode based on MesoC/PPY at applied current densities below 65 mA·cm^{-2}. Above this value, the highest values were obtained for MesoC. In all cases, C_{sp} decreases on increasing applied current density due to increasing *IR* drops, the decrease being more pronounced for MesoC/PANI, MesoC/PT and MesoC/P3MT. The values of C_{sp} obtained for the different samples are: for MesoC 77.9 F/g; for MesoC/PANI 57.6 F/g; for MesoC/PPY 83.8 F/g; for MesoC/PT 66.3 F/g and for MesoC/P3MT 52.3 F/g. Taking into account that the incorporation of the conducting polymers to the carbon surface leads to a decrease of both the specific area and the porosity of the material in all cases, the high faradaic contribution to the capacitance promoted by only 0.17% of PPY is remarkable. The low C_{sp} values obtained for MesoC/PT and MesoC/P3MT can be explained in terms of the expected higher internal resistance, as these two polymers are poorly doped in aqueous acid media. Comparing the specific capacitance data obtained in this study with those reported in the literature, it can be stated that these are of the same order or slightly lower to that previously reported for capacitors based on Monarch 1400 [33], carbon/PANI [34-36], carbon/PPY [34, 37] and carbon/polythiophenes [8, 38].

From the discharge process, the equivalent series resistance (*ESR*) of the supercapacitor cell can be estimated according to

$$ESR = \frac{\Delta V_1}{2I} \quad (2)$$

where ΔV_1 is a voltage drop, I is the applied current, and 2 is a factor due to the polarity change. Coulombic efficiency of the supercapacitor cells can be estimated as

$$E_f = \left(\frac{C_{discharge}}{C_{charge}}\right) \cdot 100 = \left(\frac{t_d}{t_c}\right) \cdot 100 \quad (3)$$

where $C_{\text{discharge}}$ and t_d stand for discharge capacitance and discharge time, respectively, and C_{charge} and t_c stand for charge capacitance and charge time, respectively [39]. Calculated internal resistance and coulombic efficiency values are shown in Table 3.

Table 3. Values of the internal resistance (ESR) and coulombic efficiency (E_f) vs. applied current density.

	Applied current density (mA·cm^{-2})											
	1		5		10		15		20		25	
Electrode	ESR (Ω)	E_f (%)	ESR (Ω)	E_f (%)	ESR (Ω)	E_f (%)	ESR (Ω)	E_f (%)	ESR (Ω)	E_f (%)	ESR (Ω)	E_f (%)
MesoC	1.84	92.4	1.59	94.2	1.34	97.5	1.50	98.2	1.56	97.3	1.56	98.2
MesoC/PANI	8.14	90.7	8,80	95.6	8.37	98.1	8.50	95.1	8.79	96.5	7.81	97.0
MesoC/PPY	2.75	89.3	2.14	94.1	2.38	97.6	3.09	96.8	2.76	98.0	-	-
MesoC/PT	15.84	59.9	8.36	76.4	16.56	88.2	9.27	91.4	-	-	-	-
MesoC/P3MT	7.98	55.0	8.15	75.4	8.55	90.0	13.49	93.6	12.59	92.2	-	-

The lowest *ESR* values correspond to MesoC. The increase of the *ESR* for the composite electrodes is being ascribed to the lower electrical conductivity of the polymers compared to the carbon conductivity. The highest *ESR* is being obtained for MesoC/PT. In all cases there is no relation between the *ESR* value and the applied current density. Regarding the coulombic efficiency, again the highest values were obtained for MesoC, but the difference decreases with increasing current densities. In all cases, E_f increases for increasing applied current density until reaching an almost constant value for current densities above 15 mA·cm^{-2}.

The cycling performance of the symmetric electrochemical capacitors was evaluated using galvanostatic charge/discharge over 7500 cycles at a current density of 25 mA·cm^{-2}. Figure 6 depicts the relationship:

$$(C_n/C_1)\cdot 100 \quad (4)$$

where C_n is the specific capacity of the n^{th} cycle (F·g^{-1}) and C_1 the specific capacity of the first cycle.

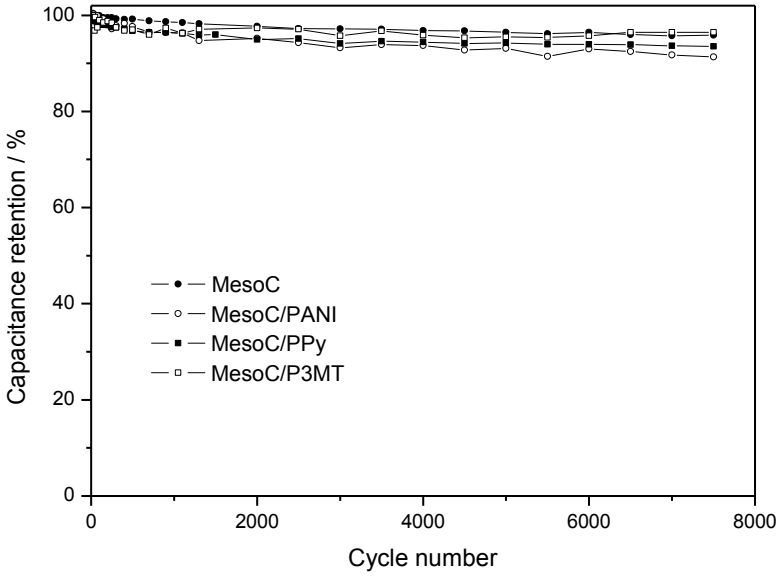

Figure 6. Dependence of relative capacitance with cycle number. Applied current density 25 mA·cm^{-2}.

From the experimental data presented in Figure 6, a total loss of about 4% of the initial discharge capacitance is found after 7500 cycles for the MesoC-based capacitor. Devices based on MesoC/PANI and MesoC/PPY electrodes show a loss of about 8.5 and 6.5 % of the initial capacitance values, while the capacitor based on MesoC/P3MT shows a loss of 3.5 %, lower than that for MesoC only. These results indicate that these three capacitors maintained a fairly stable capacitance after 7500 charge/discharge cycles at an applied current density of 25 mA·cm^{-2}. The cyclability of the capacitor based on MesoC/PT could not be determined because of its low discharge times, well below those measured for the other composites.

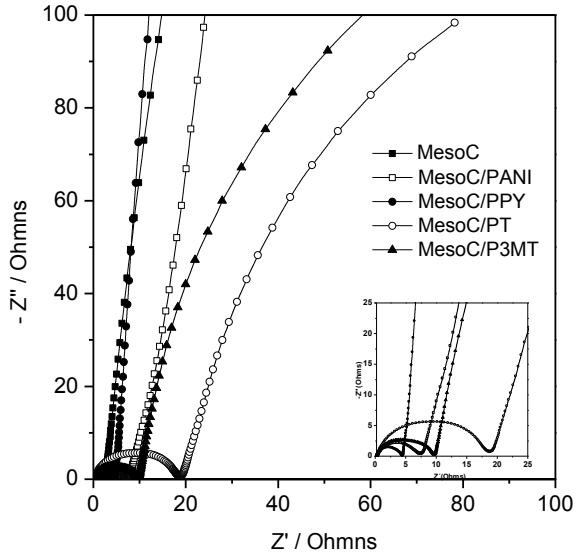

Figure 7. Nyquist diagrams of mesoporous carbon and carbon/conducting polymer based electrochemical capacitors. Perturbation amplitude 0.01 V and frequency range 5·10^{5} to 5E^{-4} Hz.

Electrochemical impedance spectroscopy (EIS) was employed to monitor the electrochemical behavior of the electrodes. The impedance spectra were measured for all capacitors with amplitude of 10 mV in a frequency range of from 500 kHz to 50 mHz. Results are shown as Nyquist plots in Figure 7. The spectra show depressed semicircles at high frequency range corresponding to bulk RC response, and a spike at low frequencies related to the charging mechanism. All devices show a deviation from the 90º line associated to pure capacitance, due to electrochemical effects such as the diffusive resistivity of the electrolyte within the pore of the electrode, as well as the surface roughness and non-uniform active layer thickness [33].

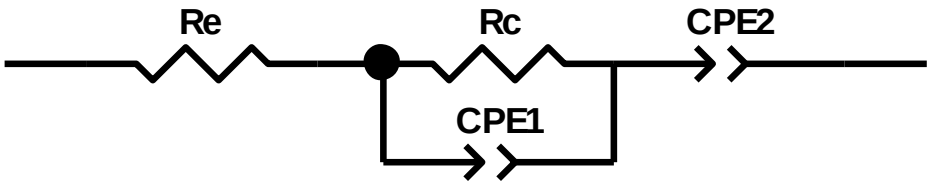

Figure 8. Scheme of the equivalent circuits proposed for the electrochemical capacitor cells.

The equivalent circuit proposed to fit the experimental impedance spectra was constructed by the following elements (Figure 8): an ohmic electrolyte resistance, R_e; a parallel subcircuit (R_c-CPE_1) that accounts for the impedance arc, and consists of a charge transfer resistance and a constant phase element representing double layer capacitance; and a low-frequency constant phase element (CPE_2), that accounts for the low frequency spike observed in the impedance plot, and includes the redox capacitance and diffusional effects for porous materials. Results obtained by fitting the experimental spectra to the equivalent circuit, using ZView software, are shown in Table 4. Ohmic electrolyte resistance is of the order of 0.2 Ω, similar in all cases. CPE_1 shows values of the order of 10^{-4} to 10^{-5} F, with relatively low values for the power (n_1~0.8) indicating non-ideal capacitance. The charge transfer resistance has values between 2 and 17 Ω. Resistance values can be compared to the ESR, since for porous electrodes the ESR is equal to the sum of all resistances in the system [33]. It is observed that total resistance and ESR values correspond in order and magnitude, with MesoC < MesoC/PPY < MesoC/PANI <. MesoC/PT < MesoC/P3MT. CPE_2 shows values from 0.54 to 1.30 F, with high values for n_2, indicating near-ideal capacitance. The highest capacitance value is obtained for MesoC/PPY cells, which coincides with results obtained from the galvanostatic charge/discharge tests.

Comparing the values of C_{sp} obtained from EIS with those obtained from galvanostatic cycles, it is observed that the values obtained from EIS are slightly lower, but tendencies are similar. Values from EIS are: MesoC 63.06 $F \cdot g^{-1}$; MesoC/PANI 31.36 $F \cdot g^{-1}$; MesoC/PPY 75.40 $F \cdot g^{-1}$, MesoC/PT 56.82 $F \cdot g^{-1}$, MesoC/P3MT 56.14 $F \cdot g^{-1}$. Both methods indicate that MesoC/PPy has highest specific capacitance, followed by MesoC. Lowest specific capacitance was found for MesoC/PT and MesoC/Pani.

Table 4. Fitted values of equivalent circuit elements from impedance spectra.

Electrode material	R_e / Ω	R_c / Ω	CPE_1 / F		CPE_2 / F	
			Q_1/ F	n_1	Q_2/ F	n_2
MesoC	0.18	2.36	$2.61.10^{-4}$	0.765	1.07	0.923
MesoC/PANI	0.29	7.46	$2.02.10^{-4}$	0.750	0.542	0.861
MesoC/PPY	0.23	4.38	$4.94.10^{-5}$	0.898	1.304	0.959
MesoC/PT	0.30	17.64	$1.31.10^{-4}$	0.807	0.964	0.814
MesoC/P3MT	0.23	8.83	$1.25.10^{-4}$	0.812	0.963	0.816

4. CONCLUSIONS

Mesoporous carbon/conducting polymer composites have been synthesized by adsorption of different monomers (aniline, pyrrole, thiophene and 3-methyltiophene) in the gas phase onto the surface of the mesoporous carbon substrate, followed by oxidative chemical polymerization. The amount of polymer in the composite material is low (between 0.2 and 3.4%).

The textural analysis of the composites examined by applying Dubinin–Radushkevich, α-plot and Kruk–Jaroniec–Sayari methods to the low temperature N_2-adsorption isotherms, show that the incorporation of the polymers to the carbon leads to a decrease of the BET surface value and the pore volume, without altering the pore size distribution, independently of the polymer nature and concentration. Electrochemical performance of the composites was studied by cyclic voltammetry, galvanostatic charge/discharge, and electrochemical impedance spectroscopy measurements in 2.0 mol l^{-1} H_2SO_4.

All composite electrodes show a stable cycle life in the potential range of 0 to 1V, the specific capacitance of MesoC/PPY composite electrode (83.8 $F \cdot g^{-1}$ as determined from charge/discharge, 75.4 $F \cdot g^{-1}$ as determined from EIS) being slightly higher than that obtained for the pristine MesoC electrode (77.9 $F \cdot g^{-1}$ as determined from charge/discharge, 63.0 $F \cdot g^{-1}$ as determined from EIS). The other composites show lower specific capacitance than pristine carbon due to their higher internal resistance (ESR). Electrochemical impedance spectroscopy results indicate that cells based on MesoC, MesoC/PANI and MesoC/PPY electrodes show the expected behavior, with a semicircle at high frequencies follow by and spike at low frequencies, while the MesoC/PT and MesoC/P3MT show double semicircles, due to the low electrical conductivity of both polymers when doped in aqueous media.

ACKNOWLEDGEMENTS
This work was supported by the Spanish Plan Nacional de Investigación Científica y Desarrollo Tecnológico Ref: ENE-2007-62791, AECI student grant, CONACYT (México) student grant 173568

and CONACYT project 47066 and 116157. We also thank Dr. T. Centeno of the Instituto Nacional del Carbón of CSIC for his collaboration in the characterization of textural properties.

References

1. B.E. Conway, *Electrochemical Supercapacitors*, Kluwer Academic/Plenum, New York (1999).
2. S. Sarangapani, B.V. Tilak, C.-P. Chen, *Journal of The Electrochemical Society* 143 (1996) 3791.
3. A.F. Burke, T.C. Murphy, In: D.H. Goughtly, B. Vyas, T. Takamura, J.R. Huff, Editors, *Materials for Energy Storage and Conversion: Batteries, Capacitors and Fuel Cells*, Materials Research Society, Pittsburgh (1995), p.375.
4. C. Arbizzani, M. Mastragostino, B. Scosati, *Handbook of Organic Conductive Molecules and Polymers*, Wiley, Chichester, UK (1997).
5. M. Jayalakshmi, K. Balasubramanian, *International Journal of Electrochemical Science* 3 (2008) 1196.
6. E. Frackowiak, *Physical Chemistry, Chemical Physics* 9 (2007) 1774
7. E. Frackowiak, F. Béguin, *Carbon* 39 (2001) 937.
8. A.Laforgue, P. Simon, C. Sarrazin, J.-F. Fauvarque, *Journal of Power Sources* 80 (1999) 142.
9. K. Jurewicz, S. Delpeux, V. Bertagna, F. Béguin, E. Frackowiak, *Chemical Physics Letters* 347 (2001) 36.
10. M. Mastragostino, C. Arbizzani, F. Soavi, *Journal of Power Sources* 97-98 (2001) 812.
11. E. Raymundo-Pinero, V. Khomenko, E. Frackowiak, F. Beguin, *Journal of The Electrochemical Society* 152 (2005) A229.
12. M. Toupin, T. Brousse, D. Bélanger, *Chemistry of Materials* 16 (2004) 3184.
13. N.-L. Wu, *Materials Chemistry and Physics* 75 (2002) 6.
14. J.P. Zheng, P.J. Cygan, T.R. Jow, *Journal of The Electrochemical Society* 142 (1995) 2699.
15. A.Burke, *Electrochimica Acta* 53 (2007) 1083.
16. V. Ruiz, R. Santamaría, M. Granda, C. Blanco, *Electrochimica Acta* 54 (2009) 4481.
17. F. Lufrano, P. Staiti, *International Journal of Electrochemistry Science* 5 (2010) 903
18. R. Ryoo, S.H. Joo, S. Jun, *The Journal of Physical Chemistry B* 103 (1999) 7743.
19. B.E. Conway, V. Birss, J. Wojtowicz, *Journal of Power Sources* 66 (1997) 1.
20. M. Mastragostino, C. Arbizzani, F. Soavi, *Solid State Ionics* 148 (2002) 493.
21. J.M. Miller, B. Dunn, *Langmuir* 15 (1999) 799.
22. M. Toupin, T. Brousse, D. Belanger, *Chemistry of Materials* 14 (2002) 3946.
23. K. Jurewicz, K. Babel, A. Ziólkowski, H. Wachowska, *Electrochimica Acta* 48 (2003) 1491.
24. M. Kodama, J. Yamashita, Y. Soneda, H. Hatori, S. Nishimura, K. Kamegawa, *Materials Science and Engineering B* 108 (2004) 156.
25. S. Brunauer, P.H. Emmett, E. Teller, *Journal of American Chemical Society* 60 (1938) 309.
26. M.M. Dubinin, In: D.A. Cadenhead, Editor, *Progress in Surface and Membrane Science*, Academic Press, London (1975).
27. H.F. Stoeckli, In: J.W. Patrick, Editor, *Porosity in Carbons*, Edward Arnold, London (1995).
28. J.A. Fernández, M. Arulepp, J. Leis, F. Stoeckli, T.A. Centeno, *Electrochimica Acta* 53 (2008) 7111.
29. T.A. Centeno, F. Stoeckli, *Electrochimica Acta* 52 (2006) 560.
30. J.A. Fernández, T. Morishita, M. Toyoda, M. Inagaki, F. Stoeckli, T.A. Centeno, *Journal of Power Sources* 175 (2008) 675.
31. M. Kruk, M. Jaroniec, A. Sayari, *Langmuir* 13 (1997) 6267.
32. K.S.W. Sing, D.H. Everrett, R.A.W. Haul, L. Moscow, R.A. Pierotti, J. Rouquerol, T. Siemieniewska, *Pure and Applied Chemistry* 57 (1985) 603.
33. S.R.S. Prabaharan, R. Vimala, Z. Zainal, *Journal of Power Sources* 161 (2006) 730.

34. E. Frackowiak, V. Khomenko, K. Jurewicz, K. Lota, F. Béguin, *Journal of Power Sources* 153 (2006) 413.
35. C. Wei-Chih, W. Ten-Chin, *Journal of Power Sources* 117 (2003) 273.
36. M.J. Bleda-Martínez, E. Morallón, D. Cazorla-Amorós, *Electrochimica Acta* 52 (2007) 4962.
37. B. Muthulakshmi, D. Kalpana, S. Pitchumani, N.G. Renganathan, *Journal of Power Sources* 158 (2006) 1533.
38. S.A. Hashmi, H.M. Upadhyaya, *Solid State Ionics* 152-153 (2002) 883.
39. F. Pico, C. Pecharroman, A. Ansón, M.T. Martinez, J.M. Rojo, *Journal of The Electrochemical Society* 154 (2007) A579